ACS APPLIED MATERIALS & INTERFACES

Research Article

www.acsami.org

# Paper-Based Device for Rapid Visualization of NADH Based on Dissolution of Gold Nanoparticles

Pingping Liang, Haixiang Yu, Bhargav Guntupalli, and Yi Xiao*

Department of Chemistry and Biochemistry, Florida International University, 11200 SW Eighth Street, Miami, Florida 33199, United States

Supporting Information

**ABSTRACT:** We describe a paper-based device that enables rapid and sensitive room-temperature detection of dihydronicotinamide adenine dinucleotide (NADH) via a colorimetric readout and demonstrate its value for monitoring $NAD^+$-driven enzymatic reactions. Our system is based on NADH-mediated inhibition of gold nanoparticle (AuNPs) dissolution in a $Au^{3+}$-cetyltrimethylammonium bromide (CTAB) solution. We fabricated a device consisting of a mixed cellulose ester paper featuring a wax-encircled, AuNP-coated film atop a cotton absorbent layer sandwiched between two plastic cover layers. In the absence of NADH, the $Au^{3+}$-CTAB complex dissolves the AuNP layer completely, generating a white color in the test zone. In the presence of NADH, $Au^{3+}$ is rapidly reduced to $Au^+$, greatly decreasing the dissolution of AuNPs and yielding a red color that becomes stronger at increasing concentrations of NADH. This device exploits capillary force-assisted vertical diffusion, allowing us to apply a 25 $\mu$L sample to a surface-confined test zone to achieve a detection limit of 12.5 $\mu$M NADH. We used the enzyme glucose dehydrogenase as a model to demonstrate that our paper-based device can monitor $NAD^+$-driven biochemical processes with and without selective dehydrogenase inhibitors by naked-eye observation within 4 min at room temperature in a small sample volume. We believe that our paper-based device could offer a valuable and low-cost analytical tool for monitoring $NAD^+$-associated enzymatic reactions and screening for dehydrogenase inhibitors in a variety of testing contexts.

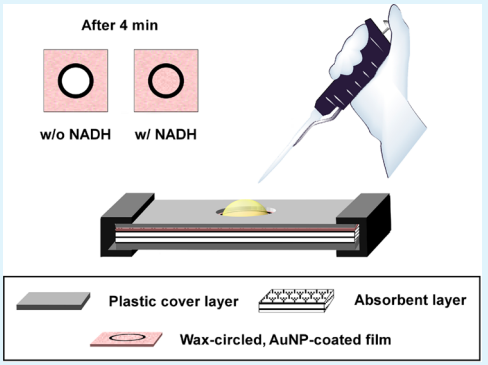


**KEYWORDS:** *dissolution of gold nanoparticles, dihydronicotinamide adenine dinucleotide, paper-based device, colorimetric screening, dehydrogenase inhibitors, $NAD^+$-driven enzymatic reactions*

## INTRODUCTION

Gold nanoparticles (AuNPs) have been widely used for applications in sensing, catalysis, imaging, diagnostics, therapy, and drug delivery due to their unique optical and electronic properties and good biological compatibility.[1−7] The properties of AuNPs usually depend on their size and shape,[8−12] and the dissolution of gold has proven to be a powerful way to resize or reshape these particles.[13] This is typically achieved by dissolving AuNPs via chemical reactions in which standard combinations of ligand/oxidant,[14−19] such as $CN^-/O_2$,[17,18,20] have been used in either an aqueous[14,15] or nonaqueous medium.[16] However, ambient $O_2$ is difficult to control as an oxidant, and the process is time-consuming.

Recently, mild oxidation of AuNPs has been achieved using solutions containing a surfactant, such as cetyltrimethylammonium bromide (CTAB).[19,21,22] Aguirre et al. first observed that exposure to CTAB in aqueous solutions enabled reshaping of gold shells to form highly asymmetric gold rod- or beanlike structures at room temperature.[23] Rodriguez-Fernandez et al. subsequently reported the sculpting of Au nanospheres via oxidation of AuNPs in $Au^{3+}$-CTAB solution, and proposed that the charged CTAB micelles spatially directed the oxidation of nanoparticles.[21] Other groups have since applied gold dissolution for the resizing or reshaping of gold nanorods (AuNRs).[13,24] More recently, the oxidative etching of AuNPs or AuNRs has been employed in nonaggregation-based colorimetric sensors for the detection of $Fe^{3+}$, $Cu^{2+}$, $Cr^{6+}$, $Pb^{2+}$, $H_2O_2$, HCl, $NO_2^-$, and $I^-$.[15,25−33] Detection was based on the dissolution of gold nanostructures by the targets at either the area of curvature or the tip along the longitudinal direction, generating a blue shift in surface plasmon resonance (SPR) absorption and a visible color change from bluish-green or red to light red and then to colorless as the target concentration increased. However, incubation for more than 5 h at high temperature (50−70 °C) is often required to observe the color change, and so far, only inorganic targets have been used with these sensor platforms.

Dihydronicotinamide adenine dinucleotide (NADH) and its oxidized form, nicotinamide adenine dinucleotide ($NAD^+$), are ubiquitous biomolecules associated with cellular energy metabolism in both eukaryotic and prokaryotic organisms.[34] It has been reported that the $NAD^+$/NADH couples are

Received: May 13, 2015
Accepted: June 22, 2015
Published: June 22, 2015





DOI: 10.1021/acsami.5b04104
ACS Appl. Mater. Interfaces 2015, 7, 15023−15030

essential cofactors for more than 300 dehydrogenase enzymes.[35,36] Increased activity of dehydrogenases, such as aldehyde dehydrogenases, has been reported in various human cancers[37] and has been found to interfere with certain chemotherapeutic treatments.[38,39] Accordingly, dehydrogenase inhibitors have been developed for the treatment of human diseases,[37,38,40] as well as applications in alcohol dependence,[41] cocaine addiction,[42] anxiety,[43] and as resensitizing agents for cancers.[44] Thus, the development of sensitive and specific NADH sensors[45,46] could not only open numerous possibilities for dehydrogenase characterization but also for screening to identify inhibitors of dehydrogenases for the development of novel anticancer agents,[47] antibiotics,[48] and pesticides.[49]

We report here a paper-based device that employs NADH-prohibited dissolution of an AuNP film to colorimetrically visualize the presence of NADH within 4 min at room temperature in a sample volume of 25 $\mu$L. In the absence of NADH, a solution containing complexes of $Au^{3+}$-CTAB completely dissolves the AuNP coating, yielding a white readout within the wax-circled test zone (Figure 1A). In the presence of NADH, $Au^{3+}$ is rapidly reduced to $Au^{+}$, which is unable to dissolve AuNPs. As the NADH concentration increases, the decreased dissolution of AuNPs results in a distinctive color readout that shifts from light pink (Figure 1B, partial dissolution of AuNPs) to red (Figure 1C, no dissolution of AuNPs) in the test zone. We used the enzyme glucose dehydrogenase (GDH) to evaluate the potential of this paper-based colorimetric device to monitor $NAD^{+}$-driven biochemical processes in the presence or absence of inhibitors. This testing platform therefore offers users the ability to rapidly and sensitively screen inhibitors of GDH based on their modulation of the $NAD^{+}$-driven enzymatic reaction by the naked eye using a mechanism that is most likely generalizable to hundreds of different dehydrogenase enzymes.

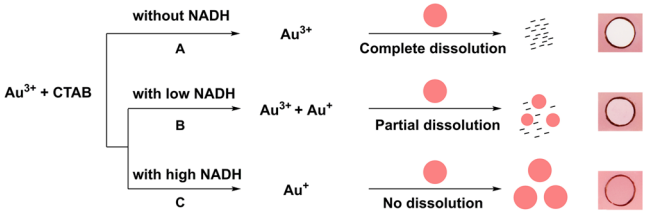


**Figure 1.** Colorimetric NADH visualization with a paper-based sensor. Citrate-coated AuNPs (4.4 ± 1.6 nm diameter) are deposited on mixed cellulose ester (MCE) filter paper via ambient vacuum filtration, forming a red AuNP-coated layer. (A) In the absence of NADH, $Au^{3+}$-CTAB completely dissolves the AuNP coating, yielding a white readout. (B) In the presence of 50 $\mu$M NADH, partial reduction of $Au^{3+}$ by NADH results in only partial dissolution of AuNPs, resulting in a light pink color. (C) When challenged with 200 $\mu$M NADH, all of the $Au^{3+}$ is reduced by NADH, leaving the AuNPs intact and producing a red readout.

## RESULTS AND DISCUSSION

It has been previously reported that AuNPs dissolve in an acidic $Au^{3+}$-CTAB solution,[21] and we recently discovered that NADH could inhibit this dissolution at room temperature. Therefore, we sought to use $Au^{3+}$-CTAB dissolution of AuNPs as the basis for a colorimetric NADH sensor. To achieve a short reaction time, we used the AuNPs with smaller diameters as the signaling reporter because they can be dissolved faster.[21,50] Citrate-capped AuNPs were synthesized as previously reported[51] and then concentrated to 2.67 $\mu$M. The particles were characterized by transmission electron microscopy (TEM), and the analysis of image confirmed that the AuNPs are uniform with a diameter of ~4.4 ± 1.6 nm (Supporting Information (SI), Figure S1). AuNP dissolution requires a CTAB concentration that is greater than its critical micelle concentration[52] to form micelles that carry $Au^{3+}$ ions. When we added 160 nanomoles of $Au^{3+}$ to a 44.4 mM CTAB solution (pH 4.0), the $Au^{3+}$-CTAB complex—more specifically, the $AuBr_4^-$ anion—exhibited strong absorbance at 394 nm with a distinct shoulder at 450 nm, as predicted.[53] Upon adding 328 picomoles of AuNPs, we found that the plasmon peak of the AuNPs shifted from 504 to 526 nm in the $Au^{3+}$-CTAB solution. The absorbance of both the $Au^{3+}$-CTAB complex at 394 nm and the AuNPs at 526 nm gradually decreased over the course of the reaction (SI, Figure S2A). Under reaction conditions where the $Au^{3+}$:AuNP ratio was 489:1, we found that the absorbance at 526 nm decreased very rapidly in the first 10 min and started to reach a plateau after 40 min. We did not observe any detectable change after 60 min, clearly indicating that all AuNPs were dissolved (SI, Figure S2B). In contrast, we observed no dissolution of AuNPs in CTAB solution without $Au^{3+}$ and used this as a reference to calculate the relative absorbance decrease at 526 nm.

The concentration of $Au^{3+}$ plays an important role in AuNP dissolution. We therefore optimized the $Au^{3+}$:AuNP ratio in a homogeneous solution to achieve a much shorter reaction time. Specifically, we prepared samples by adding different concentrations of $Au^{3+}$ to identical aliquots of AuNPs and allowing the reaction to progress for 40 min. After the reaction, we recorded the UV−vis spectra. The results showed that AuNP dissolution increased along with the $Au^{3+}$ concentration. Compared with AuNPs alone, the absorbance at 526 nm was greatly decreased but still detectable when the $Au^{3+}$ concentration was in the range of 40−160 $\mu$M (SI, Figure S3). As the $Au^{3+}$ concentration increased to 200 $\mu$M (an $Au^{3+}$:AuNP ratio of 610:1), the particle plasmon peak completely disappeared, indicating that all of the AuNPs were dissolved. It is clear that a high concentration of $Au^{3+}$ promotes quick dissolution of AuNPs at room temperature, and we therefore used an $Au^{3+}$:AuNP ratio of 610:1 in subsequent experiments.

$Au^{3+}$ can dissolve AuNPs in an acidic CTAB solution, whereas its reduced form ($Au^{+}$) is unable to perform such dissolution.[21] Xiao et al. previously reported that NADH facilitates the rapid reduction of $Au^{3+}$ to $Au^{+}$ in CTAB solution,[54] and we therefore predicted that the presence of NADH would inhibit the dissolution of AuNPs in a $Au^{3+}$-CTAB solution. To confirm this, we investigated the effect of different concentrations of NADH on AuNP dissolution by monitoring absorbance at 526 nm (SI, Figure S4A). At concentrations below 75 $\mu$M, NADH reduced only a small quantity of $Au^{3+}$ to $Au^{+}$, and the excess $Au^{3+}$ remaining in the solution was sufficient to dissolve most of the AuNPs. The absorbance of the small quantity of AuNPs remaining in the solution under these conditions became difficult to measure accurately due to strong interference from the distinct shoulder of the $Au^{3+}$-CTAB complex at 450 nm. When the NADH concentration was in the range of 100−150 $\mu$M, the amount of unreacted $Au^{3+}$ in the solution only allowed for partial dissolution of AuNPs to occur. AuNP dissolution was further inhibited at increasing NADH concentrations; interestingly, we observed a higher AuNP absorbance after 40 min upon


DOI: 10.1021/acsami.5b04104
ACS Appl. Mater. Interfaces 2015, 7, 15023−15030

addition of 240 $\mu$M NADH relative to the absorbance of undissolved AuNPs. This is because the excess NADH first fully reduced $Au^{3+}$ to $Au^{+}$ and then further reduced $Au^{+}$ to $Au^{0}$. This resulted in the enlargement of the AuNPs, consistent with previously reported findings.[54] By monitoring the absorbance change at 526 nm, we could identify NADH concentrations above 75 $\mu$M (SI, Figure S4B).

To achieve detection in an instrument-free manner, we transferred the NADH-inhibited dissolution process onto mixed cellulose ester (MCE) filter paper. The uniform pore size of MCE paper allows stable and reproducible liquid flow through the membrane, and a smooth and even AuNP layer can be rapidly formed on the MCE surface via simple vacuum filtration. We used this routine lab technique to prepare the AuNP-coated film because previous work has shown that films made by this technique generally offer good homogeneity, strong adhesive strength, massive scalability, excellent stability, and reproducibility.[55,56] We fabricated our films by filtering 1.9 mL of freshly made, citrate-capped AuNPs (771.4 picomoles of particles) on MCE paper. After drying for 20 min at room temperature, we cut the film into 20 squares (~21 picomoles AuNPs on each piece; 5 mm W × 6 mm L) and dropped these squares into $Au^{3+}$-CTAB solutions containing different concentrations of NADH. We observed that a 200 $\mu$M $Au^{3+}$-CTAB solution dissolved all of the AuNPs from the surface in the absence of NADH, leaving the paper a white color (Figure 2). The amount of $Au^{3+}$ in the solution decreased with

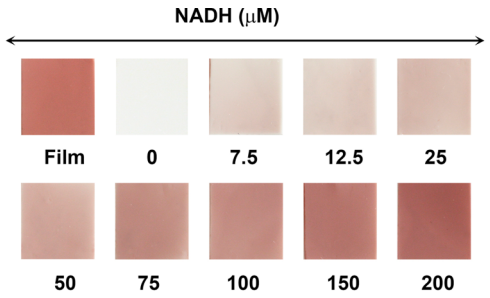


**Figure 2.** Colorimetric detection of NADH on AuNP-coated mixed cellulose ester (MCE) filter paper. Increasing the NADH concentration from 0 to 200 $\mu$M in a 200 $\mu$M $Au^{3+}$-CTAB solution increasingly inhibited the dissolution of AuNPs coated on the paper, resulting in a stronger red color readout.

increasing NADH concentrations, inhibiting the dissolution of AuNPs coated on the paper and resulting in a color readout that shifted from light pink to red (Figure 2). Time-course experiments with AuNP-coated squares in 200 $\mu$M $Au^{3+}$-CTAB solution indicated that the dissolution of AuNPs increased with an increase in the reaction time (SI, Figure S5). Although it took 40 min to complete the reaction, the color difference was readily detectable via naked-eye observation with a detection limit of 7.5 $\mu$M, 10-fold lower than the reported value of a solution-based colorimetric NADH sensor.[54]

We subsequently optimized the design of our paper-based sensor to further shorten the reaction time, making it possible to visualize the presence of NADH in a microliter-scale sample. To work with very small sample volumes on the AuNP-coated film, we needed to be able to confine the sample within the test zone to avoid the lateral escape of reactants. The best way to achieve such confinement is to create both a closed hydrophobic barrier on the surface of the AuNP-coated film and an underlying hydrophobic wall across the thickness of the paper. This can be done via wax printing, a rapid and inexpensive technique for the large-scale production of microfluidic paper-based analytical devices.[57] However, wax printing requires a time-consuming heat penetration step and is generally difficult to form a good hydrophobic barrier across the thickness of the paper.[57] As a simple alternative, we formed a hydrophobic barrier on the surface by using a wax pencil to draw a circle on the AuNP-coated paper to confine the reactants. This wax drawing can be performed in five seconds with good reproducibility and no restriction on the thickness of the circle.

Lateral diffusion of fluids in paper is usually much more rapid than vertical diffusion.[57] When a 25 $\mu$L droplet of $Au^{3+}$-CTAB solution was placed on the AuNP-coated paper without wax confinement, we observed that a narrow white circle formed at the edge of the droplet after 10 min and that 46% of AuNPs dissolved in the reaction area (SI, Figure S6A). Most of the $Au^{3+}$-CTAB micelles, which are typically ~3 nm in diameter,[58] presumably migrated to the edge of the droplet due to the "coffee ring effect",[59] such that particles in this region are more likely to be dissolved than those in the center. In general, however, the wax circle confines the sample and allows vertical, but not lateral, diffusion of liquid out of the AuNP-coated test zone. We observed that a droplet of 25 $\mu$L $Au^{3+}$-CTAB was successfully retained within the wax-circled test zone for up to 21 min and had 58% of the AuNPs dissolved (SI, Figure S6B). However, the dissolution was still restricted primarily to the edge of the wax-circled test zone, whereas the film at the center remained intact and red. We also observed lateral escape of the confined reactants from underneath the wax barrier.

To further eliminate lateral diffusion in the confined test zone, we added a hydrophilic absorbent layer underneath the wax-circled AuNP-coated film to enhance the vertical mass transport of reactants within the paper. Because water has at least a 10-fold higher self-diffusion coefficient[60] than CTAB micelles,[61,62] water molecules travel faster than $Au^{3+}$-CTAB micelles during capillary force-assisted vertical diffusion, resulting in a greatly increased concentration of $Au^{3+}$-CTAB complex in the test zone as water is removed by this absorbent layer. When the AuNP dissolution occurred with the absorbent layer, the capillary force significantly enhanced vertical diffusion and thereby prevented the formation of the previously observed "coffee ring" reaction pattern, resulting in more uniform dissolution with a shorter reaction time (SI, Figure S7). A uniform surface reaction requires a good match between the AuNP-coated film and the absorbent layer. We tested different absorbent layers, including paper towel, Kimwipe, rice paper, copy paper, and cotton pads, and found that the most uniform dissolution of AuNPs occurred with a cotton absorbent layer (SI, Figure S7).

The homogeneity and speed of dissolution can be further improved by employing a "wet-to-wet" combination of a wax-circled AuNP-coated film and an absorbent cotton layer (SI, Figure S8). Control experiments demonstrated that 25 $\mu$L of $Au^{3+}$-CTAB solution confined in a dry AuNP-coated test zone took 9 min to dissolve 80% of the AuNPs in combination with a dry cotton layer, whereas 90% of the AuNPs were dissolved when we put a prewetted AuNP-coated film on top of a dry cotton absorbent layer. We believe that the nonuniform pattern formed on these AuNP-coated films is due to the existence of tiny air bubbles between the AuNP films and the dry cotton layer and therefore requires more time to facilitate mass transport through the film. In contrast, when we formed a tight


DOI: 10.1021/acsami.5b04104
ACS Appl. Mater. Interfaces 2015, 7, 15023−15030

contact between the layers by prewetting both the AuNP-coated film and the cotton layer, all of the AuNPs dissolved after 4 min due to uniform mass transportation.

We incorporated these various enhancements into a simple device that can achieve a uniform and rapid detection reaction from a microliter-scale sample within a surface-confined test zone. We prepared our AuNP-coated paper as above, used a wax pencil to enclose AuNP-coated reaction zones within circular barriers (5 mm diameter), and cut the film into nine 8 mm × 8 mm squares. We then assembled a device (Figure 3)

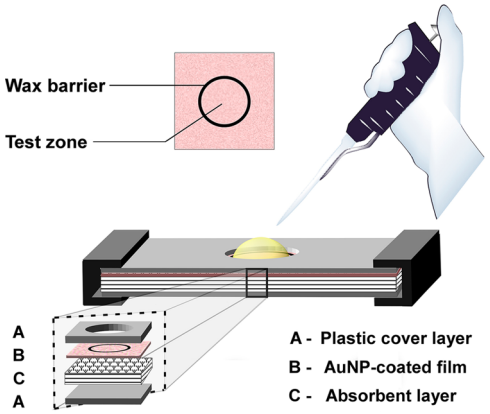


**Figure 3.** A simple paper-based device for colorimetric detection of NADH in a microliter-scale sample in <4 min. The device consists of an upper plastic cover layer with a hole exposing the test zone, a wax-circled AuNP-coated paper, a cotton absorbent layer, and a lower plastic cover layer. We added a 25 $\mu$L reaction solution to the test zone, which is confined within the wax circle on the AuNP-coated paper.

that incorporates the following layers: an uppermost plastic cover layer with a 6 mm diameter hole that exposes the test zone, a prewetted wax-circled AuNP-coated film, a prewetted cotton absorbent layer in contact with the underside of the AuNP-coated film, and a plastic cover layer at the bottom. The four layers were clamped together by clipping the edges of the device. This device allowed us to visualize the presence of NADH at room temperature (Figure 4A). The time-course demonstrated that complete dissolution of AuNPs within this device was obtained in under 4 min (SI, Figure S9). Under optimized experimental conditions, the lowest concentration of NADH that can be clearly visualized on our paper-based device is 12.5 $\mu$M. Using ImageJ software, we measured the intensity of the color in the test zone and plotted the normalized intensity for different concentrations of NADH (Figure 4B).

We anticipated that NADH-mediated inhibition of AuNP dissolution could enable simple and direct detection of dehydrogenase-driven $NAD^+$ reduction for a number of analytes. As a model, we chose GDH, an enzyme that converts $NAD^+$ into NADH in the presence of glucose, where the glucose concentration determines the amount of NADH produced.[63] Our results confirmed that NADH generated by GDH modulates the dissolution of the AuNP film in our device, generating a colorimetric readout that can be resolved within 4 min. The AuNPs in the test zone were completely dissolved in the absence of glucose, indicating that no NADH was being produced. The amount of NADH increased with increasing glucose concentrations, and the color of the test zone changed from light pink to red as the glucose concentration increased from 2 to 20 mM (Figure 5). To test the robustness of our device, we further performed the detection of NADH (SI, Figure S10) and monitored $NAD^+$-driven enzymatic reactions (Figure 5) in 20% *E. coli* cell lysate. Experimental results demonstrated that these complex sample matrices did not measurably affect our results.

Heavy metal ions, such as Ag(I) and Hg(II), are strong inhibitors of GDH, whereas Pb(II) has been reported to have no inhibitory effect on the GDH reaction.[64] To demonstrate the ability of this device to screen for enzyme inhibitors, we tested the effects of Ag(I), Hg(II), and Pb(II) on GDH-driven NADH production. In the presence of 20 $\mu$M or higher Ag(I), the activity of GDH was completely inhibited and no NADH was generated, yielding a completely white readout (Figure 6, Ag(I)). GDH activity was also significantly inhibited by 20 $\mu$M Hg(II), although the enzyme still generated a very small amount of NADH that resulted in ~30% inhibition of AuNP dissolution, yielding a light pink color in the test zone. Clearly, the GDH inhibition and AuNP dissolution was increased with increasing Hg(II) concentration, completely dissolving AuNP in the test zone at a $Hg^{2+}$ ion concentration of 100 $\mu$M (Figure 6, Hg(II)). As expected, we did not observe any dissolution of AuNPs in the test zone in the presence of Pb(II) at concentrations ranging between 20 and 100 $\mu$M (Figure 6,

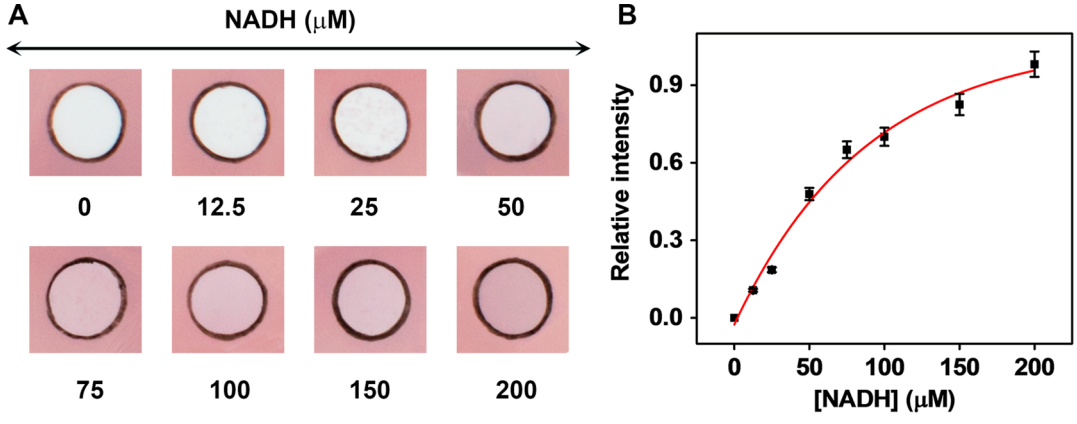


**Figure 4.** Successful detection of NADH in 25 $\mu$L samples in under 4 min at room temperature on a paper-based device. (A) We tested multiple concentrations of NADH in 200 $\mu$M $Au^{3+}$-CTAB solution. (B) Test zone readouts were measured with ImageJ software, and the relative intensity was calculated by normalizing the unreacted AuNP-coated film to 1 and the AuNP-coated film in the absence of NADH to 0.


DOI: 10.1021/acsami.5b04104
ACS Appl. Mater. Interfaces 2015, 7, 15023−15030

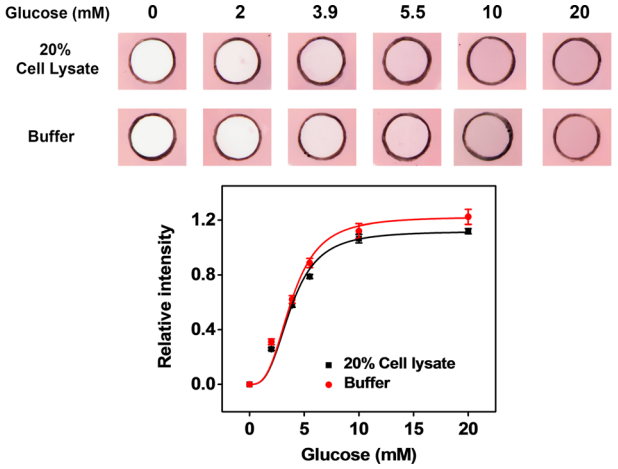


**Figure 5.** Detecting NADH production by glucose dehydrogenase (GDH) with our paper-based device at room temperature. (top) The device was used to measure NADH production by 0.1 U GDH in the presence of different concentrations (0–20 mM) of glucose in buffer or 20% cell lysate after a 4 min reaction. Because *E. coli* cell lysate contains NADH, 600 $\mu$M $Au^{3+}$-CTAB was used in 20% *E. coli* cell lysate instead of 400 $\mu$M $Au^{3+}$-CTAB in buffer to completely dissolve the AuNPs in the test zone. (bottom) The intensity of the readouts in the test zones was measured with ImageJ software, and the relative intensity was calculated by normalizing the unreacted AuNP film to 1 and the fully dissolved AuNP-coated film without glucose to 0.

Pb(II)). This confirmed that Pd(II) has no inhibitory effect on GDH, which is consistent with the literature.[64]

To demonstrate the inhibitory effects of different concentrations of Hg(II) on GDH-driven NADH-production, we further performed the enzymatic reaction with Hg(II) concentrations ranging from 0 to 200 $\mu$M. The resulting solution was then added to a 400 $\mu$M $Au^{3+}$-CTAB solution, and 25 $\mu$L of this mixture was immediately applied to the test zone. In the absence of Hg(II), GDH fully converted $NAD^+$ to NADH after 4 min, completely inhibiting AuNP dissolution and leaving the test zone dark red. In the presence of 2.5 $\mu$M Hg(II), enzyme activity was slightly inhibited, and we observed a small decrease of color intensity in the test zone. GDH-mediated production of NADH decreased in parallel with the increase of Hg(II) concentration, yielding a lighter readout as increased dissolution of AuNPs occurred (SI, Figure S11). At a Hg(II) concentration of 100 $\mu$M, we observed a completely white readout within the wax-circled test zone, indicating complete inhibition of GDH and dissolution of AuNPs (SI, Figure S11A). The color intensity was measured with ImageJ software, and we plotted the normalized intensity with different concentrations of Hg(II) (SI, Figure S11B). The activity of GDH in homogeneous solution was also monitored with different concentrations of Hg(II) (SI, Figure S12). Enzyme activity was calculated based on the kinetics of the enzymatic reaction and defined as 100% in the absence of Hg(II). On the basis of this analysis, we calculated an $IC_{50}$ value of 20 $\mu$M for this ion on our paper-based device, which is consistent with its $IC_{50}$ value obtained in homogeneous solution (18 $\mu$M) (SI, Figure S12).

## CONCLUSIONS

We have developed a paper-based colorimetric platform/device for detecting the presence of NADH based on this molecule's inhibitory effect on the dissolution of AuNPs. We further show how this system could offer a simple and inexpensive assay for monitoring $NAD^+$-dependent enzymatic reactions or for screening potential dehydrogenase inhibitors. We used vacuum filtration to fabricate a uniform AuNP-coated film on MCE paper. In the absence of NADH, $Au^{3+}$ in a CTAB solution completely dissolved the AuNPs on the film, resulting in a color change from red to bright white. In the presence of NADH, $Au^{3+}$ is rapidly reduced to $Au^+$ by NADH, and the resulting decrease in $Au^{3+}$ concentration significantly inhibits the dissolution of the AuNP layer. As NADH concentration increases, this reduced dissolution results in a colorimetric readout that shifts from light pink to red. By making use of the colorimetric change associated with NADH-inhibited dissolution of AuNPs, we subsequently incorporated this film into a paper-based device that exploits a wax-confined test zone and capillary force-assisted vertical diffusion to analyze a 25 $\mu$L sample with a detection limit of 12.5 $\mu$M under 4 min at room temperature. Importantly, the assay is also robust enough to perform the NADH detection in cell lysate.

With GDH as a model, we further demonstrate the capacity of our paper-based device for monitoring $NAD^+$-driven enzymatic reactions with and without dehydrogenase inhibitors. To show the potential usefulness of our device as a means for screening enzyme inhibitors, we utilized this paper-based device to test the inhibitory effects of Ag(I) and Hg(II) on GDH-driven NADH production. Our results confirmed that the reduced production of NADH by GDH in the presence of these heavy metal ions translates to increased dissolution of the AuNPs on our paper-based device, generating a colorimetric readout that can successfully report the extent of enzymatic

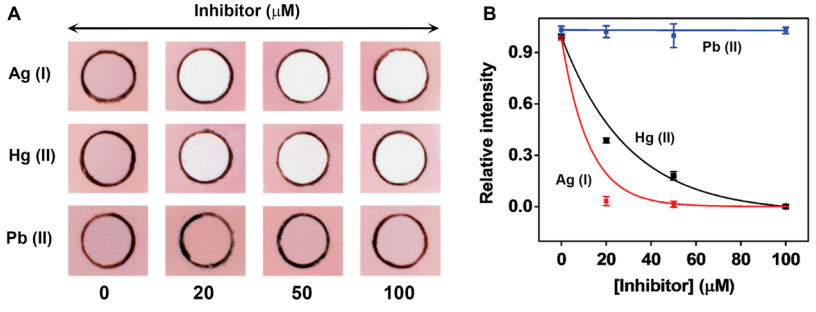


**Figure 6.** Screening the inhibitory effects of various heavy metal ions on GDH-driven NADH production. (A) Our paper-based device was used to measure NADH production by 0.1 U GDH in a 25 $\mu$L sample containing different concentrations (0–100 $\mu$M) of heavy metal ions in 400 $\mu$M $Au^{3+}$-CTAB after a 4 min reaction. (B) The intensity of the readouts in the test zones was measured with ImageJ software, and the relative intensity was calculated by normalizing the unreacted AuNP film to 1 and the fully dissolved AuNP-coated film in the presence of 100 $\mu$M Ag(I) to 0.


DOI: 10.1021/acsami.5b04104
ACS Appl. Mater. Interfaces 2015, 7, 15023–15030

inhibition by the naked eye within 4 min at room temperature in a 25 μL sample volume. Although this is only a simple proof-of-concept device designed for a single test, one could easily fabricate a device with multiple test zones, suitable for high throughput testing. We believe that our device could offer a useful analytical tool for the rapid visualization of other dehydrogenase-mediated $NAD^+$ transformations in a variety of contexts.[36,65−70]

## EXPERIMENTAL SECTION

**Chemicals.** Gold(III) chloride trihydrate, trisodium citrate dihydrate, sodium borohydride ($NaBH_4$), cetyltrimethylammonium bromide (CTAB), dihydronicotinamide adenine dinucleotide (NADH), nicotinamide adenine dinucleotide ($NAD^+$), glucose, glucose dehydrogenase (from *Pseudomonas* sp.), mercury(II) acetate, lead(II) acetate trihydrate, silver nitrate, tryptone, sodium chloride (NaCl), yeast extract, and phosphate buffer solution (1.0 M, pH 7.4) were purchased from Sigma-Aldrich and used as received. All solutions were prepared with Milli-Q water. Wild type *E. coli* strain K12 was used for detection in cell lysate.

**Synthesis of AuNPs.** AuNPs (4 nm) were synthesized by adding 0.5 mL of 0.01 M $HAuCl_4$ and 0.5 mL of 0.01 M trisodium citrate solution to 18 mL of deionized water with stirring. We then added 0.5 mL of ice-cold, freshly prepared 0.1 M $NaBH_4$ solution to the solution and immediately stopped stirring. At this point, the solution turned orange-red.[51] The newly synthesized AuNPs were used within 2−5 h of preparation. The concentration of AuNPs was determined based on their extinction coefficient constant with a UV−vis spectrometer (Cary 100, Varian). Particle size was characterized by TEM (JEOL JEM 2100 LaB6).

**Optimization of AuNP Dissolution in Solution.** To observe the dissolution of AuNPs in the $Au^{3+}$-CTAB solution, we used an Amicon Ultra Centrifugal Filter (Millipore) to concentrate the as-prepared AuNPs at 1500 rcf (Eppendorf 5430R), obtaining a 6.6-fold concentrated solution of AuNPs. We then added 328 picomoles of concentrated AuNPs to a 44.4 mM CTAB solution (pH 4) containing 160 nanomoles of $Au^{3+}$ and recorded the UV−vis spectra for an hour at room temperature. The dissolution was very fast during the first 10 min and started to reach its plateau after 40 min. To test the effects of $Au^{3+}$ concentration on AuNP dissolution, we added 0−200 μM gold salt in CTAB solution to identical aliquots of gold nanoparticles (328 picomoles) and incubated for 40 min at room temperature while recording the UV−vis spectra. We also tested the AuNP dissolution with solutions containing different concentrations of NADH, which were freshly prepared before use. We mixed these with a 200 μM gold salt solution and then added 328 picomoles AuNPs to this mixture and recorded the UV−vis spectra of samples after 40 min at room temperature.

**Fabrication and Testing of AuNP-Coated Film.** MCE membrane substrate (Millipore, 47 mm diameter, 100 nm pore size, and 100-μm thickness) was prewetted with deionized water on a Kontes 47 mm Ultra-Ware Microfiltration support base (Kimble Chase). A 1.9 mL (771.4 picomoles) freshly made, citrate-capped AuNP solution diluted with 3.1 mL of 256 μM sodium citrate was added to the funnel, and we subsequently prepared the film via ambient vacuum filtration. The film was then cut into 20 small pieces (5 mm W × 6 mm L) after air-drying for 20 min, resulting in strips of film each coated with 21 picomoles AuNPs. These were dropped into 200 μM $Au^{3+}$-CTAB solution containing different concentrations of NADH and then photographed with a Nikon D800 after 40 min.

**NADH Detection with a Paper-Based AuNP Colorimetric Device.** After preparing the film, we used a wax pencil (Phano China Marker, Fisher Scientific) to draw circles (5 mm diameter) on the AuNP-coated film. The film was then cut into 9 pieces (8 mm W × 8 mm L). We fabricated a device with four layers, listed here from top to bottom: a polyvinyl chloride plastic cover layer (4.4 cm W × 5.4 cm L) with a 6 mm diameter hole on the top, a prewetted, wax-circled AuNP-coated filter paper, a prewetted layer of hydrophilic cotton absorbent padding with Kimwipe paper, and a bottom plastic cover. The four layers were clamped together by clipping the edges of the device with paper clips. Twenty-five microliters of 200 μM $Au^{3+}$-CTAB solution containing different concentrations of NADH was added to the wax circled reaction zone, and the color change was visualized after 4 min. Intensity analysis was performed with ImageJ software (http://imagej.nih.gov/ij/).

**GDH-Directed NADH Production and the Inhibition Effect of Heavy Metal Ions on GDH.** We combined 0.1 U GDH with different concentrations (0−20 mM) of glucose in 0.1 M phosphate buffer solution (pH 7.4) at 25 °C for 30 min, mixed this with 400 μM $Au^{3+}$-CTAB, and applied the mixture to the paper-based device for a 4 min reaction. To test the inhibitory effects of Hg(II), we incubated different concentrations of Hg(II) with 0.1 U GDH for 10 min in the presence of 10 mM glucose and 0.1 M phosphate buffer solution (pH 7.4) at 25 °C and then added 6 mM $NAD^+$ to initiate the enzymatic reaction for 15 min. The kinetics of the reaction were monitored for the first 6 min in a microplate reader to calculate the enzyme's activity. Ten microliters of the enzymatic reaction solution were added to 90 μL of 400 μM $Au^{3+}$-CTAB solution, and 25 μL of this solution was applied to the device test zone. We visualized the colorimetric results after 4 min and evaluated the inhibitory effects of these metals by measuring the decrease in the color intensity produced by the enzyme−substrate reaction. We also tested Ag(I) and Pb(II) as potential inhibitors in a similar fashion. Intensity analysis was performed with ImageJ software.

**Detection of NADH and GDH-Directed NADH Production in 20% Cell Lysate.** Wild type *E. coli* strain K-12 was cultured in 50 mL of autoclaved L-broth (Luria) media (10 g/L tryptone, 5 g/L yeast extract, and 10 g/L NaCl) in an Erlenmeyer flask and was harvested after 24 h of incubation at 37 °C with orbital shaking. We obtained an optical density ($OD_{600}$) reading of 1.62 with an approximate cell density of $1.62 \times 10^9$ cells/mL. The resultant cell suspension was centrifuged at 8500*g* for 15 min at 4 °C. Pelleted cells were resuspended in 1.62 mL of 0.1 M phosphate buffer solution (pH 7.4). The cells were lysed with a Misonix Microson XL2000 ultrasonic cell disruptor for a 10 s pulse with 30 s intervals 4 times in an ice-water bath. The lysate was centrifuged at 5000*g* for 10 min at 4 °C. The final decanted supernatant was diluted with phosphate buffer (0.1 M, pH 7.4) to make a 20% (v/v) cell lysate (~$1 \times 10^{10}$ cells/mL). The detection of NADH and GDH-directed NADH production were performed as described above except the reaction buffer was replaced with 20% cell lysate.

## ASSOCIATED CONTENT

### Supporting Information

Characterization of synthesized AuNPs; time course of AuNP dissolution in $Au^{3+}$-CTAB solution; the effect of $Au^{3+}$ concentration on AuNP dissolution in CTAB; the effect of NADH concentration on AuNP dissolution; time course of NADH on AuNP-coated mixed cellulose ester (MCE) filter paper in the absence and presence of NADH in $Au^{3+}$-CTAB solution; lateral diffusion limits AuNP dissolution due to reactant escape either with or without a wax-circled test zone; performance of dry versus wet wax-circled films in conjunction with a dry or wet cotton absorbent layer; time course of NADH in 25 μL samples at room temperature on a paper-based device in the absence and presence of NADH in $Au^{3+}$-CTAB solution; detecting NADH with and without cell lysate using our paper-based device at room temperature; detection of Hg(II)-mediated inhibition of GDH-driven $NAD^+$-reduction at different concentrations; and inhibition of Hg(II) on the activity of GDH in homogeneous solution. The Supporting Information is available free of charge on the ACS Publications website at DOI: 10.1021/acsami.5b04104.



DOI: 10.1021/acsami.5b04104
ACS Appl. Mater. Interfaces 2015, 7, 15023−15030

## AUTHOR INFORMATION


### Corresponding Author

*E-mail: yxiao2@fiu.edu.


### Notes

The authors declare no competing financial interest.

## ACKNOWLEDGMENTS

This work was supported by Start-Up Funds from Florida International University. We thank Dr. Zhihong Nie and his student Zhiqi Huang from University of Maryland (College Park) for obtaining high-resolution TEM images of AuNPs.

## REFERENCES


(1) Jain, P. K.; El-Sayed, I. H.; El-Sayed, M. A. Au Nanoparticles Target Cancer. *Nano Today* **2007**, *2*, 18−29.

(2) Medley, C. D.; Smith, J. E.; Tang, Z. W.; Wu, Y. R.; Bamrungsap, S.; Tan, W. H. Gold Nanoparticle-Based Colorimetric Assay for the Direct Detection of Cancerous Cells. *Anal. Chem.* **2008**, *80*, 1067−1072.

(3) Ghosh, P.; Han, G.; De, M.; Kim, C. K.; Rotello, V. M. Gold Nanoparticles in Delivery Applications. *Adv. Drug Delivery Rev.* **2008**, *60*, 1307−1315.

(4) El-Sayed, I. H.; Huang, X. H.; El-Sayed, M. A. Surface Plasmon Resonance Scattering and Absorption of Anti-EGFR Antibody Conjugated Gold Nanoparticles in Cancer Diagnostics: Applications in Oral Cancer. *Nano Lett.* **2005**, *5*, 829−834.

(5) Murphy, C. J.; Gole, A. M.; Stone, J. W.; Sisco, P. N.; Alkilany, A. M.; Goldsmith, E. C.; Baxter, S. C. Gold Nanoparticles in Biology: Beyond Toxicity to Cellular Imaging. *Acc. Chem. Res.* **2008**, *41*, 1721−1730.

(6) Jain, S.; Hirst, D. G.; O'Sullivan, J. M. Gold nanoparticles as Novel Agents for Cancer Therapy. *Br. J. Radiol.* **2012**, *85*, 101−113.

(7) Saha, K.; Agasti, S. S.; Kim, C.; Li, X. N.; Rotello, V. M. Gold Nanoparticles in Chemical and Biological Sensing. *Chem. Rev.* **2012**, *112*, 2739−2779.

(8) Link, S.; El-Sayed, M. A. Size and Temperature Dependence of the Plasmon Absorption of Colloidal Gold Nanoparticles. *J. Phys. Chem. B* **1999**, *103*, 4212−4217.

(9) Henglein, A. Physicochemical Properties of Small Metal Particles in Solution: "Microelectrode" Reactions, Chemisorption, Composite Metal Particles, and the Atom-to-Metal Transition. *J. Phys. Chem.* **1993**, *97*, 5457−5471.

(10) Valden, M.; Lai, X.; Goodman, D. W. Onset of Catalytic Activity of Gold Clusters on Titania with the Appearance of Nonmetallic Properties. *Science* **1998**, *281*, 1647−1650.

(11) Pan, Y.; Neuss, S.; Leifert, A.; Fischler, M.; Wen, F.; Simon, U.; Schmid, G.; Brandau, W.; Jahnen-Dechent, W. Size-Dependent Cytotoxicity of Gold Nanoparticles. *Small* **2007**, *3*, 1941−1949.

(12) Qian, K.; Sweeny, B. C.; Johnston-Peck, A. C.; Niu, W.; Graham, J. O.; Duchene, J. S.; Qiu, J.; Wang, Y. C.; Engelhard, M. H.; Su, D.; Stach, E. A.; Wei, W. D. Surface Plasmon-Driven Water Reduction: Gold Nanoparticle Size Matters. *J. Am. Chem. Soc.* **2014**, *136*, 9842−9845.

(13) Sreeprasad, T. S.; Samal, A. K.; Pradeep, T. Body- or Tip-Controlled Reactivity of Gold Nanorods and Their Conversion to Particles through Other Anisotropic Structures. *Langmuir* **2007**, *23*, 9463−9471.

(14) Pal, T.; Jana, N. R.; Sau, T. K. Nucleophile Induced Dissolution of Gold. *Corros. Sci.* **1997**, *39*, 981−986.

(15) Tripathy, S. K.; Woo, J. Y.; Han, C. S. Highly Selective Colorimetric Detection of Hydrochloric Acid Using Unlabeled Gold Nanoparticles and an Oxidizing Agent. *Anal. Chem.* **2011**, *83*, 9206−9212.

(16) Praharaj, S.; Panigrahi, S.; Basu, S.; Pande, S.; Jana, S.; Ghosh, S. K.; Pal, T. Effect of Bromide and Chloride Ions for the Dissolution of Colloidal Gold. *J. Photochem. Photobiol., A* **2007**, *187*, 196−201.

(17) Weisbecker, C. S.; Merritt, M. V.; Whitesides, G. M. Molecular Self-Assembly of Aliphatic Thiols on Gold Golloid. *Langmuir* **1996**, *12*, 3763−3772.

(18) McCarthy, A. J.; Coleman, R. G.; Nicol, M. J. The Mechanism of the Oxidative Dissolution of Colloidal Gold in Cyanide Media. *J. Electrochem. Soc.* **1998**, *145*, 408−414.

(19) Dasog, M.; Scott, R. W. J. Understanding the Oxidative Stability of Gold Monolayer-Protected Clusters in the Presence of Halide Ions under Ambient Conditions. *Langmuir* **2007**, *23*, 3381−3387.

(20) Lou, X. D.; Zhang, Y.; Qin, J. G.; Li, Z. A Highly Sensitive and Selective Fluorescent Probe for Cyanide Based on the Dissolution of Gold Nanoparticles and Its Application in Real Samples. *Chem.—Eur. J.* **2011**, *17*, 9691−9696.

(21) Rodríguez-Fernández, J.; Pérez-Juste, J.; Mulvaney, P.; Liz-Marzán, L. M. Spatially-Directed Oxidation of Gold Nanoparticles by Au(III)-CTAB Complexes. *J. Phys. Chem. B* **2005**, *109*, 14257−14261.

(22) Goulet, P. J. G.; Leonardi, A.; Lennox, R. B. Oxidation of Gold Nanoparticles by Au(III) Complexes in Toluene. *J. Phys. Chem. C* **2012**, *116*, 14096−14102.

(23) Aguirre, C. M.; Kaspar, T. R.; Radloff, C.; Halas, N. J. CTAB Mediated Reshaping of Metallodielectric Nanoparticles. *Nano Lett.* **2003**, *3*, 1707−1711.

(24) Khanal, B. P.; Zubarev, E. R. Purification of High Aspect Ratio Gold Nanorods: Complete Removal of Platelets. *J. Am. Chem. Soc.* **2008**, *130*, 12634−12635.

(25) Zou, R. X.; Guo, X.; Yang, J.; Li, D. D.; Peng, F.; Zhang, L.; Wang, H. J.; Yu, H. Selective Etching of Gold Nanorods by Ferric Chloride at Room Temperature. *CrystEngComm* **2009**, *11*, 2797−2803.

(26) Zhang, Z. Y.; Chen, Z. P.; Qu, C. L.; Chen, L. X. Highly Sensitive Visual Detection of Copper Ions based on the Shape-Dependent LSPR Spectroscopy of Gold Nanorods. *Langmuir* **2014**, *30*, 3625−3630.

(27) Liu, R. L.; Chen, Z. P.; Wang, S. S.; Qu, C. L.; Chen, L. X.; Wang, Z. Colorimetric Sensing of Copper(II) Based on Catalytic Etching of Gold Nanoparticles. *Talanta* **2013**, *112*, 37−42.

(28) Li, F. M.; Liu, J. M.; Wang, X. X.; Lin, L. P.; Cai, W. L.; Lin, X.; Zeng, Y. N.; Li, Z. M.; Lin, S. Q. Non-aggregation Based Label Free Colorimetric Sensor for the Detection of Cr (VI) Based on Selective Etching of Gold Nanorods. *Sens. Actuators, B* **2011**, *155*, 817−822.

(29) Chandrasekar, G.; Mougin, K.; Haidara, H.; Vidal, L.; Gnecco, E. Shape and Size Transformation of Gold Nanorods (GNRs) via Oxidation Process: A Reverse Growth Mechanism. *Appl. Surf. Sci.* **2011**, *257*, 4175−4179.

(30) Ni, W. H.; Kou, X. S.; Yang, Z.; Wang, J. F. Tailoring Longitudinal Surface Plasmon Wavelengths, Scattering and Absorption Cross Sections of Gold Nanorods. *ACS Nano* **2008**, *2*, 677−686.

(31) Chen, Z. P.; Zhang, Z. Y.; Qu, C. L.; Pan, D. W.; Chen, L. X. Highly Sensitive Label-Free Colorimetric Sensing of Nitrite Based on Etching of Gold Nanorods. *Analyst (Cambridge, U.K.)* **2012**, *137*, 5197−5200.

(32) Liu, J. M.; Jiao, L.; Cui, M. L.; Lin, L. P.; Wang, X. X.; Zheng, Z. Y.; Zhang, L. H.; Jiang, S. L. A Highly Sensitive Non-aggregation Colorimetric Sensor for the Determination of $I^-$ Based on its Catalytic Effect on $Fe^{3+}$ Etching Gold Nanorods. *Sens. Actuators, B* **2013**, *188*, 644−650.

(33) Chen, Y. Y.; Chang, H. T.; Shiang, Y. C.; Hung, Y. L.; Chiang, C. K.; Huang, C. C. Colorimetric Assay for Lead Ions Based on the Leaching of Gold Nanoparticles. *Anal. Chem.* **2009**, *81*, 9433−9439.

(34) Ying, W. H. $NAD^+$/NADH and $NADP^+$/NADPH in Cellular Functions and Cell Death: Regulation and Biological Consequences. *Antioxid. Redox Signaling* **2008**, *10*, 179−206.

(35) Jaegfeldt, H.; Kuwana, T.; Johansson, G. Electrochemical Stability of Catechols with a Pyrene Side Chain Strongly Adsorbed on Graphite Electrodes for Catalytic Oxidation of Dihydronicotinamide Adenine Dinucleotide. *J. Am. Chem. Soc.* **1983**, *105*, 1805−1814.

(36) Wu, Q.; Maskus, M.; Pariente, F.; Tobalina, F.; Fernández, V. M.; Lorenzo, E.; Abruña, H. D. Electrocatalytic Oxidation of NADH at Glassy Carbon Electrodes Modified with Transition Metal Complexes




DOI: 10.1021/acsami.5b04104
*ACS Appl. Mater. Interfaces* 2015, 7, 15023−15030

Containing 1,10-Phenanthroline-5,6-dione Ligands. *Anal. Chem.* **1996**, *68*, 3688−3696.
(37) Koppaka, V.; Thompson, D. C.; Chen, Y.; Ellermann, M.; Nicolaou, K. C.; Juvonen, R. O.; Petersen, D.; Deitrich, R. A.; Hurley, T. D.; Vasiliou, V. Aldehyde Dehydrogenase Inhibitors: a Comprehensive Review of the Pharmacology, Mechanism of Action, Substrate Specificity, and Clinical Application. *Pharmacol. Rev.* **2012**, *64*, 520−539.
(38) Tanei, T.; Morimoto, K.; Shimazu, K.; Kim, S. J.; Tanji, Y.; Taguchi, T.; Tamaki, Y.; Noguchi, S. Association of Breast Cancer Stem Cells Identified by Aldehyde Dehydrogenase 1 Expression with Resistance to Sequential Paclitaxel and Epirubicin-Based Chemotherapy for Breast Cancers. *Clin. Cancer Res.* **2009**, *15*, 4234−4241.
(39) Deng, S.; Yang, X.; Lassus, H.; Liang, S.; Kaur, S.; Ye, Q.; Li, C.; Wang, L. P.; Roby, K. F.; Orsulic, S.; Connolly, D. C.; Zhang, Y.; Montone, K.; Butzow, R.; Coukos, G.; Zhang, L. Distinct Expression Levels and Patterns of Stem Cell Marker, Aldehyde Dehydrogenase Isoform 1 (ALDH1), in Human Epithelial Cancers. *PLoS One* **2010**, *5*, e10277.
(40) Robins, R. K. Nucleoside and Nucleotide Inhibitors of Inosine Monophosphate (IMP) Dehydrogenase as Potential Antitumor Inhibitors. *Nucleosides Nucleotides* **1982**, *1*, 35−44.
(41) Arolfo, M. P.; Overstreet, D. H.; Yao, L.; Fan, P.; Lawrence, A. J.; Tao, G.; Keung, W. M.; Vallee, B. L.; Olive, M. F.; Gass, J. T.; Rubin, E.; Anni, H.; Hodge, C. W.; Besheer, J.; Zablocki, J.; Leung, K.; Blackburn, B. K.; Lange, L. G.; Diamond, I. Suppression of Heavy Drinking and Alcohol Seeking by a Selective ALDH-2 Inhibitor. *Alcohol.: Clin. Exp. Res.* **2009**, *33*, 1935−1944.
(42) Yao, L.; Fan, P.; Arolfo, M.; Jiang, Z.; Olive, M. F.; Zablocki, J.; Sun, H. L.; Chu, N.; Lee, J.; Kim, H. Y.; Leung, K.; Shryock, J.; Blackburn, B.; Diamond, I. Inhibition of Aldehyde Dehydrogenase-2 Suppresses Cocaine Seeking by Generating THP, a Cocaine Use−Dependent Inhibitor of Dopamine Synthesis. *Nat. Med. (N. Y., NY, U. S.)* **2010**, *16*, 1024−1028.
(43) Overstreet, D. H.; Knapp, D. J.; Breese, G. R.; Diamond, I. A Selective ALDH-2 Inhibitor Reduces Anxiety in Rats. *Pharmacol., Biochem. Behav.* **2009**, *94*, 255−261.
(44) Hilton, J. Role of Aldehyde Dehydrogenase in Cyclophosphamide-Resistant L1210 Leukemia. *Cancer Res.* **1984**, *44*, 5156−5160.
(45) Ma, W.; Li, D. W.; Sutherland, T. C.; Li, Y.; Long, Y. T.; Chen, H. Y. Reversible Redox of NADH and $NAD^+$ at a Hybrid Lipid Bilayer Membrane Using Ubiquinone. *J. Am. Chem. Soc.* **2011**, *133*, 12366−12369.
(46) Ma, W.; Ying, Y. L.; Qin, L. X.; Gu, Z.; Zhou, H.; Li, D. W.; Sutherland, T. C.; Chen, H. Y.; Long, Y. T. Investigating Electron-Transfer Processes Using a Biomimetic Hybrid Bilayer Membrane System. *Nat. Protoc.* **2013**, *8*, 439−450.
(47) Granchi, C.; Roy, S.; Giacomelli, C.; Macchia, M.; Tuccinardi, T.; Martinelli, A.; Lanza, M.; Betti, L.; Giannaccini, G.; Lucacchini, A.; Funel, N.; Leon, L. G.; Giovannetti, E.; Peters, G. J.; Palchaudhuri, R.; Calvaresi, E. C.; Hergenrother, P. J.; Minutolo, F. Discovery of *N*-Hydroxyindole-Based Inhibitors of Human Lactate Dehydrogenase Isoform A (LDH-A) as Starvation Agents against Cancer Cells. *J. Med. Chem.* **2011**, *54*, 1599−1612.
(48) Birkenstock, T.; Liebeke, M.; Winstel, V.; Krismer, B.; Gekeler, C.; Niemiec, M. J.; Bisswanger, H.; Lalk, M.; Peschel, A. Exometabolome Analysis Identifies Pyruvate Dehydrogenase as a Target for the Antibiotic Triphenylbismuthdichloride in Multiresistant Bacterial Pathogens. *J. Biol. Chem.* **2012**, *287*, 2887−2895.
(49) Degli Esposti, M. Inhibitors of NADH−Ubiquinone Reductase: an Overview. *Biochim. Biophys. Acta* **1998**, *1364*, 222−235.
(50) Ivanova, O. S.; Zamborini, F. P. Electrochemical Size Discrimination of Gold Nanoparticles Attached to Glass/Indium-Tin-Oxide Electrodes by Oxidation in Bromide-Containing Electrolyte. *Anal. Chem.* **2010**, *82*, 5844−5850.
(51) Busbee, B. D.; Obare, S. O.; Murphy, C. J. An Improved Synthesis of High-Aspect-Ratio Gold Nanorods. *Adv. Mater. (Weinheim, Ger.)* **2003**, *15*, 414−416.
(52) Cifuentes, A.; Bernal, J. L.; Diez-Masa, J. C. Determination of Critical Micelle Concentration Values Using Capillary Electrophoresis Instrumentation. *Anal. Chem.* **1997**, *69*, 4271−4274.
(53) Mortier, T.; Persoons, A.; Verbiest, T. Oxidation of Solid Gold in Chloroform Solutions of Cetyltrimethylammonium Bromide. *Inorg. Chem. Commun.* **2005**, *8*, 1075−1077.
(54) Xiao, Y.; Pavlov, V.; Levine, S.; Niazov, T.; Markovitch, G.; Willner, I. Catalytic Growth of Au Nanoparticles by NAD(P)H Cofactors: Optical Sensors for $NAD(P)^+$-Dependent Biocatalyzed Transformations. *Angew. Chem.* **2004**, *116*, 4619−4622.
(55) Wu, Z. C.; Chen, Z. H.; Du, X.; Logan, J. M.; Sippel, J.; Nikolou, M.; Kamaras, K.; Reynolds, J. R.; Tanner, D. B.; Hebard, A. F.; Rinzler, A. G. Transparent, Conductive Carbon Nanotube Films. *Science* **2004**, *305*, 1273−1276.
(56) Lee, J. H.; Kong, B. S.; Baek, Y. K.; Yang, S. B.; Jung, H. T. Tin Nanoparticle Thin Film Electrodes Fabricated by the Vacuum Filtration Method for Enhanced Battery Performance. *Nanotechnology* **2009**, *20*, 235203.
(57) Carrilho, E.; Martinez, A. W.; Whitesides, G. M. Understanding Wax Printing: A Simple Micropatterning Process for Paper-Based Microfluidics. *Anal. Chem.* **2009**, *81*, 7091−7095.
(58) Dorshow, R.; Briggs, J.; Bunton, C. A.; Nicoli, D. F. Dynamic Light Scattering from Cetyltrimethylammonium Bromide Micelles: Intermicellar Interactions at Low Ionic Strengths. *J. Phys. Chem.* **1982**, *86*, 2388−2395.
(59) Deegan, R. D.; Bakajin, O.; Dupont, T. F.; Huber, G.; Nagel, S. R.; Witten, T. A. Capillary Flow as the Cause of Ring Stains From Dried Liquid Drops. *Nature* **1997**, *389*, 827−829.
(60) Mills, R. Self-diffusion in Normal and Heavy Water in the Range 1−45 deg. *J. Phys. Chem.* **1973**, *77*, 685−688.
(61) Lindman, B.; Puyal, M.-C.; Kamerka, N.; Rymden, R.; Stilbs, P. Micelle Formation of Anionic and Cationic Surfactants from Fourier Transform Hydrogen-1 and Lithium-7 Nuclear Magnetic Resonance and Tracer Self-Diffusion Studies. *J. Phys. Chem.* **1984**, *88*, 5048−5057.
(62) Otto, W. H.; Britten, D. J.; Larive, C. K. NMR Diffusion Analysis of Surfactant−Humic Substance Interactions. *J. Colloid Interface Sci.* **2003**, *261*, 508−513.
(63) Zhang, M. G.; Smith, A.; Gorski, W. Carbon Nanotube-Chitosan System for Electrochemical Sensing Based on Dehydrogenase Enzymes. *Anal. Chem.* **2004**, *76*, 5045−5050.
(64) Kobayashi, Y.; Horikoshi, K. Purification and Properties of NAD-Dependent D-Glucose Dehydrogenase Produced by Alkalophilic *Corynebacterium* sp. No. 93−1. *Agric. Biol. Chem.* **1980**, *44*, 2261−2269.
(65) Pariente, F.; Lorenzo, E.; Tobalina, F.; Abruna, H. D. Aldehyde Biosensor Based on the Determination of NADH Enzymatically Generated by Aldehyde Dehydrogenase. *Anal. Chem.* **1995**, *67*, 3936−3944.
(66) Teymourian, H.; Salimi, A.; Hallaj, R. Low Potential Detection of NADH Based on $Fe_3O_4$ Nanoparticles/Multiwalled Carbon Nanotubes Composite: Fabrication of Integrated Dehydrogenase-Based Lactate Biosensor. *Biosens. Bioelectron.* **2012**, *33*, 60−68.
(67) Jena, B. K.; Raj, C. R. Electrochemical Biosensor Based on Integrated Assembly of Dehydrogenase Enzymes and Gold Nanoparticles. *Anal. Chem.* **2006**, *78*, 6332−6339.
(68) Álvarez-González, M. I.; Saidman, S. B.; Lobo-Castañón, M. J.; Miranda-Ordieres, A. J.; Tuñón-Blanco, P. Electrocatalytic Detection of NADH and Glycerol by $NAD^+$-Modified Carbon Electrodes. *Anal. Chem.* **2000**, *72*, 520−527.
(69) Rao, T. N.; Yagi, I.; Miwa, T.; Tryk, D. A.; Fujishima, A. Electrochemical Oxidation of NADH at Highly Boron-Doped Diamond Electrodes. *Anal. Chem.* **1999**, *71*, 2506−2511.
(70) Narvaez Villarrubia, C. W.; Rincon, R. A.; Radhakrishnan, V. K.; Davis, V.; Atanassov, P. Methylene Green Electrodeposited on SWNTs-Based "Bucky" Papers for NADH and L-Malate Oxidation. *ACS Appl. Mater. Interfaces* **2011**, *3*, 2402−2409.


DOI: 10.1021/acsami.5b04104
*ACS Appl. Mater. Interfaces* 2015, 7, 15023−15030